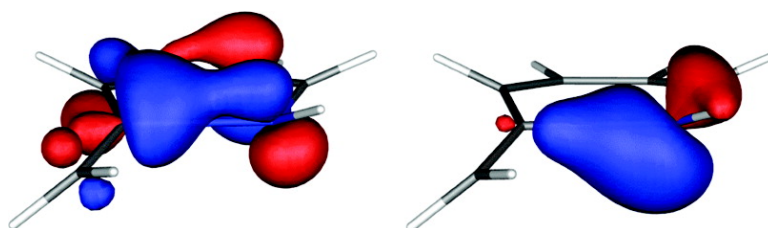Article

Secondary Orbital Effect in the Electrocyclic Ring Closure of 7-Azahepta-1,2,4,6-tetraene#A CASSCF Molecular Orbital Study

James A. Duncan, David E. G. Calkins, and Mariya Chavarha

More About This Article

Additional resources and features associated with this article are available within the HTML version:

- Supporting Information
- Access to high resolution figures
- Links to articles and content related to this article
- Copyright permission to reproduce figures and/or text from this article

View the Full Text HTML

Secondary Orbital Effect in the Electrocyclic Ring Closure of 7-Azahepta-1,2,4,6-tetraene—A CASSCF Molecular Orbital Study

James A. Duncan,* David E. G. Calkins,[†] and Mariya Chavarha[†]

*Department of Chemistry, Lewis & Clark College,
Portland, Oregon 97219-7899*

Received June 17, 2007; E-mail: duncan@lclark.edu

Abstract: Results of (10,9)CASSCF/6-31G* and B3LYP/6-31G* level calculations on the potential surface for the electrocyclic ring closure of *E*-7-azahepta-1,2,4,6-tetraene **3** to 1-aza-6-methylidenecyclohexa-2,4-diene (**4**) are reported, as well as parallel calculations on the electrocyclizations of hepta-1,2,4,6-tetraene **5**, hexa-1,3,5-triene **7**, *Z* and *E*-1-aza-1,3,5-hexatrienes **9** and **10**, and *Z*-7-azahepta-1,2,4,6-tetraene **12** for purposes of careful comparison. The **3** → **4** rearrangement has been studied computationally with density functional theory (DFT) by others, leading to disagreement over whether it is pseudopericyclic (de Lera, A. R.; Alvarez, R.; Lecea, B.; Torrado, A.; Cossío, F. P. *Angew. Chem., Int. Ed.* **2001**, *40*, 557−561; de Lera, A. R.; Cossío, F. P. *Angew. Chem., Int. Ed.* **2002**, *41*, 1150−1152) or pericyclic (Rodríguez-Otero, J.; Cabaleiro-Lago, E. *Angew. Chem., Int. Ed.* **2002**, *41*, 1147−1150). In accordance with disrotatory motion, the normal mode vectors for **TS$_{3→4}$** calculated at the (10,9)CASSCF/6-31G* level show a greater magnitude of rotation of the N1−H group relative to the N1−C2 bond being formed than in **TS$_{3→4}$** calculated at the B3LYP/6-31G* level. Furthermore, comparison of orbital correlation diagrams constructed entirely from localized complete active space (CAS) molecular orbitals (MOs) for the electrocyclizations of **3**, **5**, **7**, **9**, and **10** suggest that it is the highest occupied delocalized π-MO of **3** that is primarily responsible for σ-bond formation in **4**, not the terminal allenyl π-bond MO. However, there does appear to be a special secondary orbital effect role for the nitrogen lone-pair and hence the process is likely neither purely pericyclic nor pseudopericyclic.

Introduction

Electrocyclic reactions were first defined in a 1965 seminal paper by R. B. Woodward and Roald Hoffmann[1] as "the formation of a single bond between the termini of a linear system containing *k* π-electrons and the converse process." The importance of this paper, which explained any observed stereochemistry in these reactions, was recently celebrated with a Citation for Chemical Breakthroughs award from the Division of the History of Chemistry of the American Chemical Society. It was included among nine other pivotal papers, books, and patents in the first year of this awards program.[2]

An example of an electrocyclic reaction that has relatively recently been studied experimentally by Fernando Cossío and Angel de Lera, et al., involves the ring closure of intermediate **1**, which contains both imine and allenyl moieties, to give the isolable product **2**.[3] In this same paper, the authors explored with computational methods the mechanism of the rearrangement of 7-azahepta-1,2,4,6-tetraene **3** to methylidene-6-azacyclohexa-2,4-diene (**4**), as a model for the **1** → **2** one, at the B3LYP/6-31+G* level, comparing their results to those obtained

for the corresponding rearrangement of hepta-1,2,4,6-tetraene **5** to methylidenecyclohexa-2,4-diene (**6**).
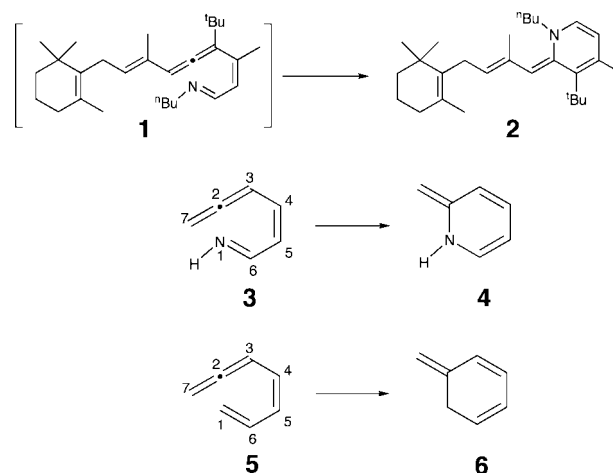
Figure 1 shows four idealized, and perhaps oversimplified, types of orbital interactions that could be involved in the **3** → **4** rearrangement. The first of the four models, model A, depicts an ordinary Woodward–Hoffmann symmetry-allowed $_{\pi}6_s$ disrotatory ring closure that is generally accepted to be involved in the rearrangement of 1,3,5-hexatriene **7** to cyclohexa-1,3-

---

[†] Lewis & Clark College undergraduate students.

(1) Woodward, R. B.; Hoffmann, R. *J. Am. Chem. Soc.* **1965**, *87*, 395–397.

(2) Wang, L. *Chem. Eng. News* **2006**, *84*, 49–50.

(3) de Lera, A. R.; Alvarez, R.; Lecea, B.; Torrado, A.; Cossío, F. P. *Angew. Chem., Int. Ed.* **2001**, *40*, 557–561.
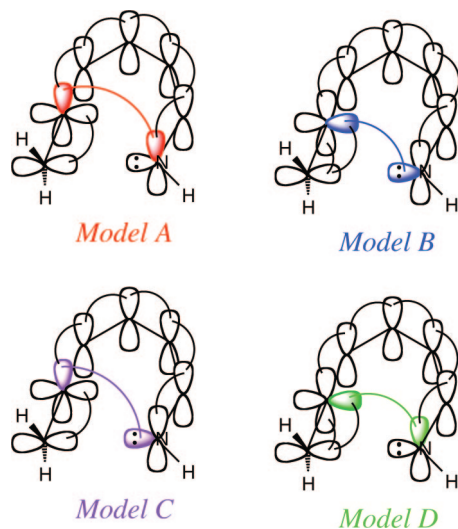
Figure 1. Possible models for the electrocyclic ring closure of **3**. Model A corresponds to an ordinary $_\pi6_s$ pericyclic process, whereas model B, model C, and model D represent pseudopericyclic alternatives.

diene (**8**), while the second, model B, depicts a pseudopericyclic[4] process with two orbital disconnections,[4d] involving the terminal allenyl π-bond and the nitrogen lone-pair orbital, both orthogonal to the rest of the π-system. In this latter model (and model D) the formal p orbital on the CH_2 moiety must rotate from overlapping with the in-plane p orbital on the allene central carbon atom in the reactant to overlap with the perpendicular central carbon p orbital in the product. Alternative formal psuedopericyclic processes with one orbital disconnection each, depicted in model C and model D of Figure 1, will be considered in context later in this paper.
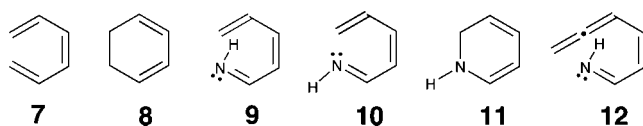
Cossío and de Lera have reported[3] that a vibrational analysis of the nuclear motion corresponding to the imaginary frequency of the transition structure for the concerted **3 → 4** rearrangement (**TS₃→₄**) calculated at the B3LYP/6-31+G* level showed no component associated with the rotation of the N1−H group relative to the N1−C2 bond being formed. The only components reportedly observed involved stretching of the forming N1−C2 bond and rotation of the exocyclic CH_2 group on the allenyl moiety. On the other hand, they report that vibrational analysis of the imaginary frequency associated with the transition structure for the corresponding **5 → 6** rearrangement (**TS₅→₆**) involves disrotatory motion as well as no significant charge redistribution. Calculated solvent effects were also found to be low for both **TS₃→₄** and **TS₅→₆**. The authors interpret these results to mean that **TS₅→₆** corresponds to an ordinary disrotatory electrocyclic rearrangement, as in model A in Figure 1, and that **TS₃→₄** corresponds to a pseudopericyclic process, presumably as depicted in model B with two orbital disconnections.

Shortly after the Cossío and de Lera paper[3] appeared, a paper by Jesús Rodriguez-Otero and Enrique Cabaleiro-Lago[5] argued that the evidence described by Cossío and de Lera was not solid enough to warrant the assertion that the **3 → 4** rearrangement is pseudopericyclic. They went on to present and interpret their own results for this rearrangement, computed at the B3LYP/6-31G** level.[6] They state that the nuclear motion corresponding to the imaginary frequency for **TS₅→₆**, the disrotatory nature of which was not in question, at least at the time, also has no component for rotation of the H_{trans}−C1 group relative to the C1−C2 bond being formed. They also suggest that it may be more illustrative of the process to focus on the rotation about the N1−C6 bond in **TS₃→₄** and **TS₅→₆**, accessed through the magnitude of the H−N1−C6−C5 and H_{trans}−C1−C6−C5 dihedral angles, respectively, and that these angles change in both **TS₃→₄** and **TS₅→₆** as the nuclear motion is animated, thus suggesting that there is rotation of the N1−C6 bond in the **3 → 4** reaction. Rodriguez-Otero and Cabaleiro-Lago also point out that if the **3 → 4** rearrangement was psuedopericyclic, then the C2−C7 bond in **TS₃→₄** should lengthen as the reaction approaches the transition state, yet transition structures **TS₃→₄** and **TS₅→₆** computed by Cossío and de Lera both have nearly identical C2−C7 short bond lengths of 1.321 and 1.326 Å, respectively, the one for **TS₃→₄** actually being slightly shorter. Thus Rodriguez-Otero and Cabaleiro-Lago concluded that the **3 → 4** reaction is a rather ordinary disrotatory electrocyclization, as they considered the **5 → 6** one to be, and not pseudopericyclic.

Then in a "Reply" Communication[7] in *Angew. Chem. Int. Ed.*, published immediately following the Rodriguez-Otero and Cabaleiro-Lago one,[5] Cossío and de Lera further argue for their contention that the **3 → 4** rearrangement is indeed pseudopericyclic. Among other arguments, they emphasize that animation of the imaginary frequency shows that attack of the NH group does not involve *significant* rotation about the N1−C6 bond and that intrinsic reaction coordinate (IRC) calculations show only marginal variations of the H−N1−C6−H dihedral angle. Both groups also present natural bond orbital analyses but their interpretations lead the two groups to opposite conclusions about whether the **3 → 4** reaction process is pseudopericyclic or not. Only the presumably most salient features of the results and arguments of Cossío et al.[3,7] and Rodriquez-Otero et al.[5] are summarized above. For full details, the reader is referred to the appropriate references.

Subsequent to the spirited exchange of interpretations in these communications, Rodriguez-Otero and Cabaleiro-Lago completed their arguments for the pericyclic nature of the rearrangement that involved both magnetic and NBO analyses in a full paper[8] and Eduardo Chamorro and Rafael Notario performed an electron localization function (ELF) analysis that supported Rodriguez-Otero's and Cabaleiro-Lago's conclusions.[9] However, Eduard Matito et al. later took exception to these results in a

(4) (a) Ross, J. A.; Seiders, R. P.; Lemal, D. M. *J. Am. Chem. Soc.* **1976**, *98*, 4325–4327. (b) Birney, D. M.; Wagenseller, P. E. *J. Am. Chem. Soc.* **1994**, *116*, 6262–6270. (c) Birney, D. M. *J. Org. Chem.* **1996**, *61*, 243–251. (d) Birney, D. M.; Ham, S.; Unruh, G. R. *J. Am. Chem. Soc.* **1997**, *119*, 4509–4517.

(5) Rodríguez-Otero, J.; Cabaleiro-Lago, E. *Angew. Chem., Int. Ed.* **2002**, *41*, 1147–1150.

(6) Although the slightly smaller 6-31G** basis set was used throughout their study,[5] it was demonstrated that geometric and energetic results, as well as activation energies, were virtually identical to results obtained with the 6-31+G* basis set.

(7) de Lera, A. R.; Cossío, F. P. *Angew. Chem., Int. Ed.* **2002**, *41*, 1150–1152.

(8) Rodríguez-Otero, J.; Cabaleiro-Lago, E. *Chem. Eur. J.* **2003**, *9*, 1837–1843.

(9) Chamorro, E. E.; Notario, R. *J. Phys. Chem. A* **2004**, *108*, 4099–4104.
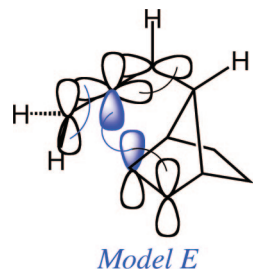
Model E

Figure 2. Model for the **13** → **15** step of the "augmented" Cope rearrangement of **13** to **14**.

Communication in the *Journal of Physical Chemistry B*[10] that was followed directly by a "Reply" Communication by Chamorro.[11] Finally, de Lera, Cossío, et al. have introduced the concept of the ellipticity of the electron density to help characterize electrocyclic reactions.[12] None of these analyses appears to be definitive with respect to whether the **3** → **4** rearrangement is pericyclic or pseudopericyclic and so the debate appears to go on.
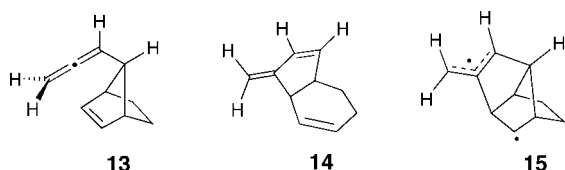
One of us has relatively recently used complete active space self-consistent field (CASSCF) calculations, in particular, to help decipher the role of the terminal allenyl C—C π-bond in a formal Cope rearrangement process.[13] CASPT2/6-31G*//CASSCF/6-31G* computations on the rearrangement of the conformationally restricted *syn*-7-allenylnorbornene (**13**) to give triene **14**[13a] showed that the reaction was nonconcerted, proceeding through diradical intermediate **15**. Two rate-determining transition structures were found between **13** and **15**, and among the bonding active space molecular orbitals for both cases were found ones that showed primarily localized internal allenyl C—C π-bonds as well as σ-bond formation that clearly shows overlap of localized terminal allenyl C—C π-bonds with a p orbital on the ring C—C double bond. Furthermore, the terminal C—C π-bond was shown to have lengthened considerably. We interpreted these facts as supporting what we termed an "augmented" Cope process, that is, one "augmented" by the extra C—C π-bond of the allenyl moiety. The essential process we envisioned is shown by model E in Figure 2 in which there is one orbital disconnection at the central carbon atom of the allenyl moiety that is similar to those exhibited by both model B and model D in Figure 1. While the latter two models are termed pseudopericyclic, we chose not use this term, but rather "augmented," for model E since the **13** → **14** rearrangement through intermediate **15** is nonconcerted.

In this paper we report the results of CASSCF and DFT calculations on the **3** → **4** rearrangement, directed toward a further understanding and delineation of the roles of the nitrogen lone-pair and the terminal allenyl C—C π-bond in the process. Our interpretation of these results is significantly influenced by the comparative results of similar calculations on the rearrangements of **5** → **6**,[14] **7** → **8**, **9** → **11**,[15] **10** → **11**,[15] **12** → **4**, a version of the **3** → **4** rearrangement in which all atoms except for the hydrogens on the CH$_2$ group were held planar, and finally a planar one in which both H—C7—C2—C3 dihedral angles were also fixed at 90°.

Computational Methodology

CASSCF calculations on all stationary points were performed using an active space consisting of six electrons in six orbitals (**7**, **8**, and **TS$_{7\rightarrow8}$**), eight electrons in seven orbitals (**9**, **10**, **11**, **TS$_{9\rightarrow11}$**, and **TS$_{10\rightarrow11}$**), eight electrons in eight orbitals (**5**, **6**, and **TS$_{5\rightarrow6}$**), or ten electrons in nine orbitals (**3**, **4**, and **TS$_{3\rightarrow4}$**). DFT calculations were carried out using the hybrid Becke[16a] three-parameter exchange functional of Lee, Yang, and Parr[16b] (B3LYP). All calculations made use of the Gaussian 98[17a] or Gaussian 03[17b] suite of programs. Appropriate vibrational analyses were also carried out, through analytical or numerical frequency calculations, to characterize stationary points as either energy minima or transition structures and to obtain zero-point energy differences.

The effects of dynamic electron correlation were included by performing CASPT2 calculations at all CASSCF stationary points using Molcas 6.4.[18] The 6-31G* basis set was used throughout for all CASSCF, CASPT2, and B3LYP calculations. Three-dimensional structural representations, including the normal mode vectors shown in Figure 3, as well as the MO representations shown in Figure 6, Figure 9, Figure 11, and in the Supporting Information section were prepared using MacMolPlt[19] with the Contour Value routinely set at 0.08.

Results and Discussion

Figure 3 shows the appropriate CASSCF/6–31G* calculated transition structures **TS$_{3\rightarrow4}$**, **TS$_{5\rightarrow6}$**, **TS$_{7\rightarrow8}$**, **TS$_{9\rightarrow11}$**, **TS$_{10\rightarrow11}$**, planar **TS$_{3\rightarrow4}$** and B3LYP/6–31G* calculated **TS$_{3\rightarrow4}$** and **TS$_{12\rightarrow4}$**, all of which exhibited a single imaginary frequency. (Coordinates and energies for these transition structures as well as those for all calculated reaction and product structures, **3–12**, are provided in Supporting Information.) As is clear from the normal mode vectors (shown in red), **TS$_{7\rightarrow8}$-(6,6)CASSCF** clearly demonstrates disrotatory motion of the CH$_2$ moieties, consistent with the conservation of orbital symmetry.[20] The H$_b$ hydrogens exhibit far more motion than the H$_a$ ones, however. In **TS$_{5\rightarrow6}$-(8,8)CASSCF** the H$_b$ motion is similar to that in **TS$_{7\rightarrow8}$-(6,6)CASSCF** (the H$_a$ motion is actually negligible) and the

(10) Matito, E.; Solà, M.; Duran, M.; Poater, J. *J. Phys. Chem. B* **2005**, *109*, 7591–7593.

(11) (a) Chamorro, E. E.; Notario, R. *J. Phys. Chem. B* **2005**, *109*, 7594–7595. Also see: Matito, E.; Poater, J.; Duran, M.; Solà, M. *ChemPhysChem* **2006**, *7*, 111–113.

(12) López, C. S.; Faza, O. N.; Cossío, F. P.; York, D. M.; de Lera, A. R. *Chem. Eur. J.* **2005**, *11*, 1734–1738.

(13) (a) Duncan, J. A.; Azar, J. K.; Beathe, J. C.; Kennedy, S. R.; Wulf, C. M. *J. Am. Chem. Soc.* **1999**, *121*, 12029–12034. (b) Duncan, J. A.; Hendricks, R. T.; Kwong, K. S. *J. Am. Chem. Soc.* **1990**, *112*, 8433–8442. (c) Duncan, J. A.; Spong, M. C. *J. Phys. Org. Chem.* **2005**, *18*, 462–467.

(14) The **5** → **6** rearrangement has also been studied extensively at the RHF level: Evanseck, J. D.; Thomas, B. E., IV; Spellmeyer, D. C.; Houk, K. N. *J. Org. Chem.* **1999**, *60*, 7134–7141.

(15) The **9** → **11** and **10** → **11** rearrangements have also been studied extensively at the B3LYP level with similar results: Walker, M. J.; Hietbrink, B. N.; Thomas, B. E., IV; Nakamura, K; Kallel, E. A.; Houk, K. N. *J. Org. Chem.* **2001**, *121*, 6669–6672.

(16) (a) Becke, A. D. *J. Chem. Phys.* **1993**, *98*, 5648–5652. (b) Lee, C.; Yang, W.; Parr, R. G. *Phys. Rev. B* **1988**, *37*, 785–789.

(17) (a) Frisch, M. J.; *Gaussian 98,* revision A.7; Gaussian, Inc.: Pittsburgh, PA, 1998. (b) Frisch, M. J.; *Gaussian 03,* revision D.01; Gaussian, Inc.: Wallingford, CT, 2004.

(18) Karlström, G.; Lindh, R.; Malmqvist, P.-Å.; Roos, B. O.; Ryde, U.; Veryazov, V.; Widmark, P.-O.; Cossi, M.; Schimmelpfennig, B.; Neogrady, P.; Seijo, L. *Comp. Mater. Sci.* **2003**, *28*, 222–239.

(19) Bode, B. M.; Gorgon, M. S. *J. Mol. Graphics Modell.* **1998**, *16*, 133–138.

(20) Woodward, R. B.; Hoffmann, R. *The Conservation of Orbital Symmetry;* Academic Press: New York, 1970.
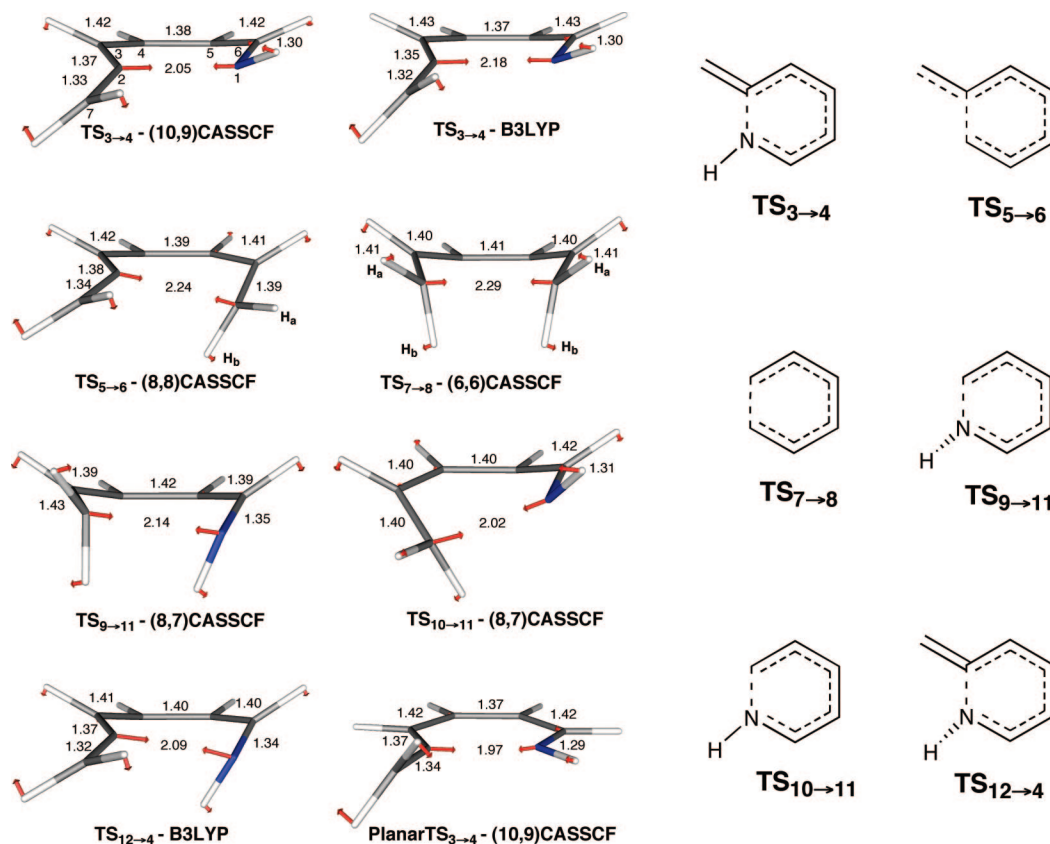
Figure 3. CASSCF/6-31* calculated transition structures **TS₃→₄**, **TS₅→₆**, **TS₇→₈**, **TS₉→₁₁**, **TS₁₀→₁₁**, **Planar TS₃→₄** and the B3LYP/6-31G* calculated **TS₃→₄** and **TS₁₂→₄**: blue color indicates nitrogen atom; carbon−carbon and carbon−nitrogen bond lengths in Å; normal mode vectors shown in red; forming σ-bonds omitted for clarity in viewing normal mode vectors. The corresponding ChemDraw structures are shown for clarity.

allenyl CH₂ moiety rotates in a way that at least on the surface of it appears consistent with overall disrotatory motion, as does the motion of hydrogen atoms on C3 and C6 of **TS₅→₆-(8,8)CASSCF**, which mimic the motion of the corresponding ones in **TS₇→₈-(6,6)CASSCF**. However, the coiled geometry conformation of **TS₅→₆-(8,8)CASSCF**, which has a C2−C4−C5-C1 dihedral angle of 14.2° (numbered as in structure **5** above), is much different than the boat geometry of **TS₇→₈-(6,6)CASS-CF** whose corresponding dihedral angle is necessarily 0.0°. The ramifications of this difference for the proper descriptions of both the **5 → 6** and **3 → 4** rearrangements, through their close comparison, is described later in this section when orbital effects are taken into consideration.

It is also observed that the normal mode vibration of **TS₉→₁₁-(8,7)CASSCF** closely resembles that of **TS₇→₈-(6,6)CASSCF** with the N1−H rotation in **TS₉→₁₁-(8,7)CASSCF** mimicking that of the Hᵦ rotation in **TS₇→₈-(6,6)CASSCF**. The vibration in **TS₁₀→₁₁-(8,7)CASSCF** also closely resembles that of **TS₇→₈-(6,6)CASSCF** except that the N1−H displacement in **TS₁₀→₁₁-(8,7)CASSCF** is greater than the Hₐ displacement in **TS₇→₈-(6,6)CASSCF**. Finally, the normal mode vibration of **TS₃→₄-(10,9)CASSCF** is consistent with the others. Its allenyl CH₂ rotation is comparable to that in **TS₅→₆-(8,8)CASSCF** and displacement of the N1−H is comparable to the displacement of Hₐ in **TS₇→₈-(6,6)CASSCF**. Thus the vibrational motion exhibited by **TS₃→₄-(10,9)CASSCF** is consistent with disrotatory motion.

As discussed above, Cossío and de Lera reported[3] that the **TS₃→₄** they obtained using B3LYP[21] showed no rotation of the N1−H group relative to the forming N1−C2 bond. As can be seen from structure **TS₃→₄-B3LYP** in Figure 3, however, a small amount of such a rotation is observed, though not of the same magnitude as observed in **TS₃→₄-(10,9)CASSCF**. Thus, at the CASSCF level, there appears to be greater disrotatory motion. **TS₉→₁₁-(8,7)CASSCF** and **TS₁₀→₁₁-(8,7)CASSCF** exhibit dis-rotatory motion as well with the N1−H of **TS₉→₁₁-(8,7)CASS-CF** behaving like Hᵦ in **TS₇→₈-(6,6)CASSCF** and the N1−H in **TS₁₀→₁₁-(8,7)CASSCF** behaving like Hₐ in **TS₇→₈-(6,6)CASS-CF**. It may be noted that the N1−C2 distance in **TS₁₀→₁₁-(8,7)CASSCF**, in which the nitrogen lone-pair is oriented in a way that it might participate in the reaction, is shorter (2.02 Å) than the corresponding N1−C2 distance in **TS₉→₁₁-(8,7)CASS-CF** (2.14 Å), where its orientation precludes it playing a role. While we were unable to study the comparable rearrangement for **12**, the Z diastereomer of **3**, at the (10,9)CASSCF level, since we were not successful in optimizing **TS₁₂→₄** with its nitrogen lone-pair in the active space, we did study it with DFT at the B3LYP/6-31G* level. **TS₁₂→₄-B3LYP**, which has a C2−C4−C5−N1 dihedral angle of 9.4° similar to the C2−C4−C5−C1 dihedral angle of 14.2° in **TS₅→₆-(8,8)CASSCF**, also exhibits motion nearly identical to that of **TS₅→₆-(8,8)CASSCF**

(21) The B3LYP structure shown in Figure 3 is one we calculated using the 6-31G* basis set. Cossío and deLera[3] calculated the transition structure for this **3 → 4** rearrangement at the B3LYP/6-31+G* level. When we repeated their calculation at this level, the structure we obtained was indistinguishable from the B3LYP/6-31G* one shown as **TS₃→₄−B3LYP** in Figure 3.

Table 1. Relative Zero-Point Corrected Enthalpy Differences, in kcal/mol, for the Stationary Points Involved in the $3 \rightarrow 4$, $5 \rightarrow 6$, $7 \rightarrow 8$, $9 \rightarrow 11$, $10 \rightarrow 11$, $12 \rightarrow 4$, and $3 \rightarrow$ **Planar TS**$_{3\rightarrow4} \rightarrow 4$ Rearrangements[a]

stationary point	relative enthalpy	stationary point	relative enthalpy	stationary point	relative enthalpy	stationary point	relative enthalpy	stationary point	relative enthalpy	stationary point	relative enthalpy	stationary point	relative enthalpy
TS$_{3\rightarrow4}$	14.3	TS$_{5\rightarrow6}$	19.2	TS$_{7\rightarrow8}$	31.7	TS$_{9\rightarrow11}$	38.6	TS$_{10\rightarrow11}$	21.4	TS$_{12\rightarrow4}$	—	**Planar**	21.1
	13.9		*20.0*		*30.3*		*37.4*		*20.7*		*24.4*	**TS$_{3\rightarrow4}$**	*18.6*
3	0	**5**	0	**7**	0	**9**	0	**10**	0	**12**	0	**3**	0
4	−31.3	**6**	−31.4	**8**	−16.0	**11**	−6.7	**11**	−6.1	**4**	—	**4**	−31.3
	−33.4		*−27.2*		*−12.5*		*−7.3*		*−7.0*		*−33.6*		*−33.4*

[a] Calculated at the appropriate CASPT2/6-31G*//CASSCF/6-31G* (regular type) and B3LYP/6-31G* (*italics*) levels (cf. Figure 3).

with the displacement of N1−H in the former comparable to that of H$_b$ in the latter, a fact discussed later in this section. Perhaps surprisingly, however, the N1−C2 bond distance in **TS**$_{12\rightarrow4}$**-B3LYP** (2.09 Å), in which the nitrogen lone-pair may not participate in bonding, is shorter than the corresponding bond distance in **TS**$_{3\rightarrow4}$**-B3LYP** (2.18 Å). Finally, Figure 3 includes the structure **Planar TS**$_{3\rightarrow4}$**-(10,9)CASSCF**, in which all atoms, except for the hydrogen atoms on the CH$_2$ group, were constrained to be planar during optimization. The discussion of its possible significance is deferred until near the end of this section.

The relative zero-point corrected enthalpy differences for the stationary states involved in the $3 \rightarrow 4$, $5 \rightarrow 6$, $7 \rightarrow 8$, $9 \rightarrow 11$, $10 \rightarrow 11$, and $12 \rightarrow 4$ rearrangements, calculated at the appropriate CASPT2/6-31G*//CASSCF/6-31G* and/or B3LYP/6-31G* levels, are given in Table 1. All rearrangements are found to be exothermic and CASPT2//CASSCF and B3LYP values compare favorably, though activation enthalpies, which differ by only 0.4−1.4 kcal/mol (except in the case of the hypothetical planar TS), compare more favorably than reaction enthalpies in most cases.
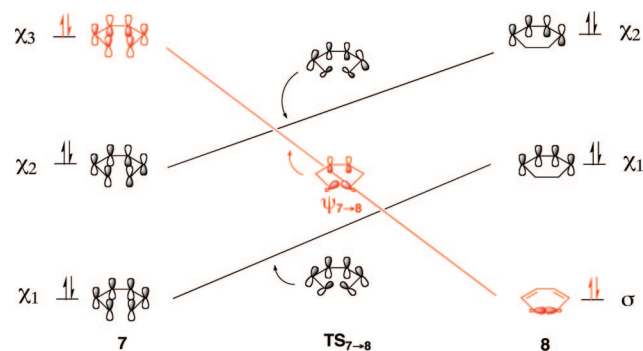
In the discussion that immediately follows, B3LYP/6-31G* energies will be given in parentheses following CASPT2/6-31G*//CASSCF/6-31G* ones, unless otherwise noted. The presence of the allene moiety in **TS**$_{3\rightarrow4}$ and **TS**$_{5\rightarrow6}$ lowers their activation enthalpies relative to **TS**$_{10\rightarrow11}$ and **TS**$_{7\rightarrow8}$ by 7.1 (6.8) and 12.5 (10.3) kcal/mol, respectively. The activation enthalpy for the formation of **TS**$_{10\rightarrow11}$, in which the nitrogen lone-pair orbital can participate, is 17.2 (16.7) kcal/mol lower than it is for the formation of **TS**$_{9\rightarrow11}$, in which the nitrogen lone-pair is directed away from the bonding site.[22] Exothermicity should not be a major contributor to activation enthalpies in this case, in a Hammond postulate sense, since the difference in reaction enthalpy for the $9 \rightarrow 11$ and $10 \rightarrow 11$ rearrangements is a rather negligible 0.6 (0.3) kcal/mol. Thus this 17.2 (16.7) activation enthalpy difference may perhaps be primarily attributed to pseudopericyclic character involving an orbital disconnection at N1 in **TS**$_{10\rightarrow11}$. Further evidence of pseudopericyclic character may be found in the C−N bond lengths. In **TS**$_{9\rightarrow11}$**-(8,7)CASSCF** the C−N bond length is 1.35 Å whereas in **TS**$_{10\rightarrow11}$**-(8,7)CASSCF** it is shorter at 1.31 Å, showing less participation of the C−N π-bond in the latter case where the N lone-pair may participate.

In addition, the activation enthalpy for the $7 \rightarrow 8$ rearrangement is 6.9 (7.1) kcal/mol lower than it is for the $9 \rightarrow 11$ one, where **TS**$_{7\rightarrow8}$ and **TS**$_{9\rightarrow11}$ have similar geometries, steric constraints, and where the only major difference between them is the C−N π-bond in the latter versus a C−C π-bond in the former. Thus if only the C−N π-bond in **TS**$_{3\rightarrow4}$, and not the nitrogen lone-pair, were to participate in stabilizing it, one might expect **TS**$_{3\rightarrow4}$ to be higher in energy than **TS**$_{5\rightarrow6}$ by about 7 kcal/mol as well. Instead it is lower by 4.9 (6.1) kcal/mol. This energy lowering of 11.8 (13.2) kcal/mol is similar to the 17.2 (16.7) kcal/mol difference calculated for the formation of **TS**$_{9\rightarrow11}$ versus **TS**$_{10\rightarrow11}$ and could perhaps also be attributed to pseudopericyclic character involving an orbital disconnection at N1 in **TS**$_{3\rightarrow4}$ and/or to less steric crowding in the $3 \rightarrow 4$ rearrangement relative to the $5 \rightarrow 6$ one. While the C2−C4−C5−N1 dihedral angles in **TS**$_{3\rightarrow4}$ and **TS**$_{7\rightarrow8}$ are nearly identical (−0.6° and 0.0°, respectively), the C2−C4−C5−C1 dihedral angle of **TS**$_{5\rightarrow6}$ (14.2°) is substantially larger than the 8.0° one in **TS**$_{9\rightarrow11}$. Such geometrical differences appear to have important consequences for the orbital analysis presented below.

Finally, the B3LYP calculated activation enthalpy difference for the formation of **TS**$_{3\rightarrow4}$ versus **TS**$_{12\rightarrow4}$ is 10.5 kcal/mol and, again, exothermicity cannot be much of a factor in this difference since the B3LYP reaction enthalpy difference for the $3 \rightarrow 4$ and $12 \rightarrow 4$ rearrangements is only 0.1 kcal/mol. This 10.5 kcal/mol activation enthalpy difference for the formation of **TS**$_{3\rightarrow4}$ versus **TS**$_{12\rightarrow4}$ is indeed very similar to the 11.8 (13.2) kcal/mol activation difference calculated for the $9 \rightarrow 11$ and $10 \rightarrow 11$ rearrangements.[22] In addition, the C−N bond length in **TS**$_{3\rightarrow4}$**-B3LYP** (1.30 Å) lengthens less than in **TS**$_{12\rightarrow4}$**-B3LYP** (1.34 Å), as was the case with **TS**$_{9\rightarrow11}$ versus **TS**$_{10\rightarrow11}$. These facts lend more credence for the involvement of an orbital disconnection at N1 (pseudopericyclic character) in the $3 \rightarrow$ **TS**$_{3\rightarrow4}$ $\rightarrow 4$ rearrangement.

Further insight into the mechanism of the $3 \rightarrow 4$ rearrangement may be obtained from a careful analysis and comparison of active space orbital correlation diagrams for the $3 \rightarrow 4$, $5 \rightarrow 6$, $7 \rightarrow 8$, $9 \rightarrow 11$, and $10 \rightarrow 11$ electrocyclizations (Figures 4, 5, 7, 8, and 10). In Figure 4 we first summarize some of the CASSCF results for the prototypical $7 \rightarrow 8$ rearrangement in terms of a type of orbital correlation diagram involving the active space molecular orbitals (MOs) we obtained for **7**, **8**, and **TS**$_{7\rightarrow8}$. For ease of viewing, the MOs are depicted in schematic ("cartoon") form. Furthermore, the contributions of the formal atomic orbitals (AOs) in the MOs of reactant **7** and product **8** are shown as equal for simplicity. The actual MOs can be found in Supporting Information. In the center of the diagram are shown similar schematic representations of the active space MOs calculated for the transition structure **TS**$_{7\rightarrow8}$. This time the relative contributions of the AOs are shown but only very approximately. Again, the actual MOs are provided in Supporting Information.

(22) A more direct comparison of the energies of **TS**$_{3\rightarrow4}$ and **TS**$_{12\rightarrow4}$ as well as **TS**$_{9\rightarrow11}$ and **TS**$_{10\rightarrow11}$ may be done in terms of their energy differences relative to products **4** and **11**, respectively, instead of based on the activation enthalpies calculated with respect to reactants **3**, **12**, **9**, and **10**. This leads to a B3LYP enthalpy difference between **TS**$_{3\rightarrow4}$ and **TS**$_{12\rightarrow4}$ of 10.7 kcal/mol (as opposed to 10.5 kcal/mol). It also leads to a CASPT2//CASSCF enthalpy difference between **TS**$_{9\rightarrow11}$ and **TS**$_{10\rightarrow11}$ of 17.8 kcal/mol (as opposed to 17.2 kcal/mol based on activation enthalpies) and a B3LYP one of 17.0 kcal/mol (as opposed to 16.7 kcal/mol based on activation enthalpies).
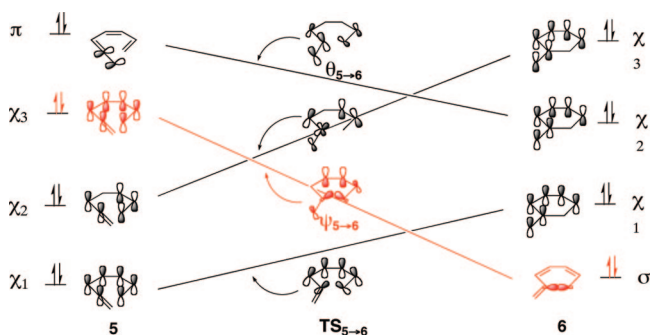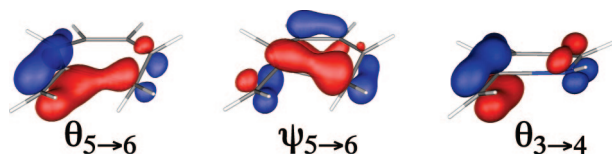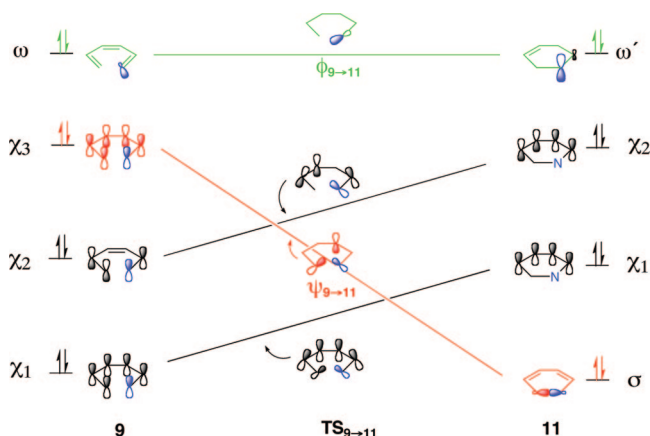
Figure 4. Orbital correlation diagram involving the (6,6)CASSCF-calculated active space bonding MOs for the concerted **7 → 8** rearrangement through **TS$_{7→8}$**. Key correlation is shown in red.

Figure 5. Orbital correlation diagram involving the (8,8)CASSCF-calculated active space bonding MOs for the concerted **5 → 6** rearrangement through **TS$_{5→6}$**. Key correlation is shown in red.


Figure 6. Transition structure active space MOs key for understanding the **5 → 6** rearrangement and its comparison with the **3 → 4** one.

Figure 7. Orbital correlation diagram involving the (8,7)CASSCF-calculated active space bonding and nonbonding MOs for the concerted **9 → 11** rearrangement through **TS$_{9→11}$**. Position of nitrogen is shown in blue, and key correlations are shown in red and green.

The three lines correlate the bonding MOs of **7** and **8** in this thermally allowed $_\pi 6_s$ disrotatory electrocyclic process and can be seen to be the only correlations possible if the phases of the MOs involved are to be preserved between reactant and product.
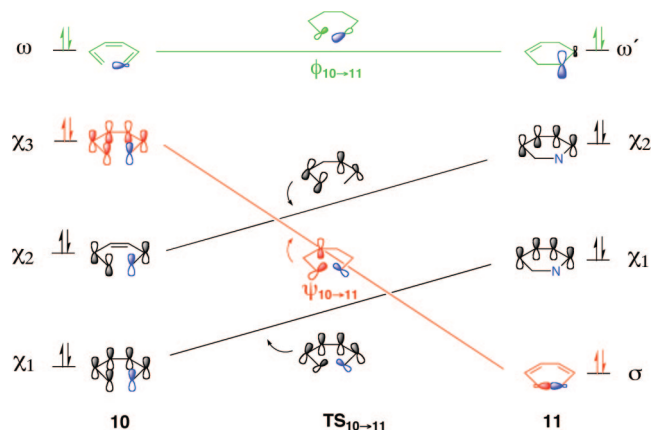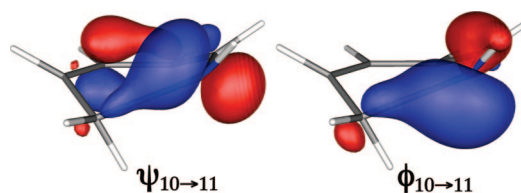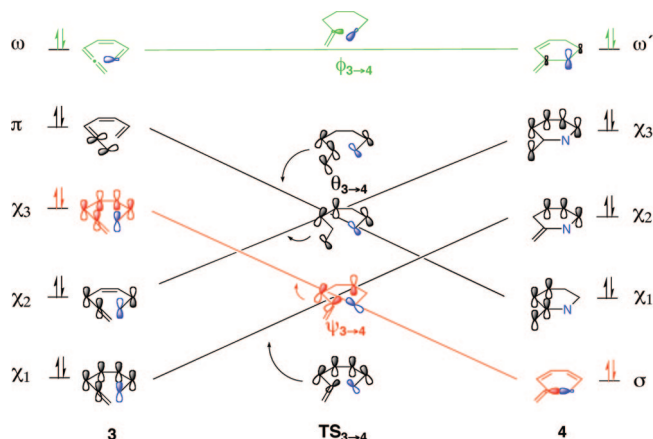

Figure 8. Orbital correlation diagram involving the (8,7)CASSCF-calculated active space bonding and nonbonding MOs for the concerted **10 → 11** rearrangement through **TS$_{10→11}$**. Position of nitrogen is shown in blue, and key correlations are shown in red and green.
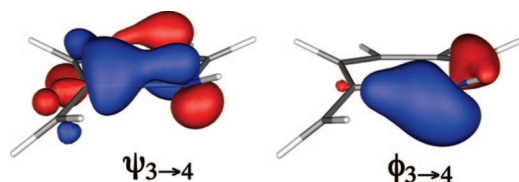

Figure 9. Key transition structure active space MOs calculated for the **10 → 11** rearrangement (cf. Figure 8). $\psi_{10→11}$ and $\phi_{10→11}$ essentially correspond to model A and model C of Figure 1, respectively (minus the terminal allenyl carbon−carbon π-bonds).

Figure 10. Orbital correlation diagram involving the (10,9)CASSCF-calculated active space bonding and nonbonding MOs for the concerted **3 → 4** rearrangement through **TS$_{3→4}$**. Position of nitrogen is shown in blue, and key correlations are shown in red and green.

As can also be seen in Figure 4, each active space MO for **TS$_{7→8}$** nicely corresponds to one and only one correlation line when necessary orbital phasing is taken into account. Thus, for example, the electrons in MOs χ_3 and $\psi_{7→8}$, highlighted in red, can be construed as providing the electrons for σ-bond formation in product **8** (σ-MO). To conserve space, the corresponding antibonding correlations are omitted. These also show that each active space MO for **7** and **8** are correlated with one unique **TS$_{7→8}$** active space antibonding MO. A complete and full page correlation diagram that shows all bonding and antibonding active space orbitals is included with the Supporting Information.

Through careful examination of all of the active space MOs, we were able to construct similar correlation diagrams for the

Figure 11. Key transition structure active space MOs calculated for the $3 \rightarrow 4$ rearrangement (cf. Figure 10). $\psi_{3 \rightarrow 4}$ and $\phi_{3 \rightarrow 4}$ essentially correspond to model A and model C of Figure 1, respectively.

$5 \rightarrow 6$, $9 \rightarrow 11$, $10 \rightarrow 11$, and $3 \rightarrow 4$ rearrangements. Full orbital correlation diagrams can be found in Supporting Information and those involving bonding and nonbonding active space orbitals are shown in Figures 5, 7, 8, and 10. (In Figures 7, 8, and 10, the position of the nitrogen is indicated in blue.) Again, the correlation lines are the only ones that make sense and each such line can be assigned a unique TS active space orbital.[23]

The orbital correlation diagram for the $5 \rightarrow 6$ rearrangement is shown in Figure 5. The generally accepted view holds that this rearrangement is, like the $7 \rightarrow 8$ one, a rather ordinary $_\pi 6_s$ pericyclic and disrotatory electrocyclic process as depicted in the π-orbital part of model A in Figure 1 (with CH$_2$ replacing the NH) for similar compound **3**.[24] However the results of this (8,8)CASSCF calculation appear to show that a more intricate explanation is warranted. As mentioned above, the conformation of **TS$_{5 \rightarrow 6}$-(8,8)CASSCF** is a coiled one in which the $\theta_{5 \rightarrow 6}$ orbital, shown schematically in Figure 5 and fully in Figure 6, appears to involve overlap of the bottom of an allyl orbital on C7–C2–C3 with the top of the p orbital on C1. Thus the $5 \rightarrow 6$ electrocyclization appears to exhibit at least some of the character of a $[_\pi 6_s + _\pi 2_a]$[25] (or equivalently a $[_\pi 6_a + _\pi 2_s]$) pseudopericyclic process[26] involving the terminal or exocyclic carbon–carbon π-bond in the process, though the exocyclic carbon–carbon bond length at 1.34 Å is only slightly longer than the 1.32 Å value typical of an allene. Such a process may be depicted in terms of model D in Figure 1. Also, however, the electrons in the delocalized π-system and not the terminal allenyl C–C π-bond can be construed as formally forming the σ bond in **6**, that is a χ_3 (of **5**) to σ-MO transition through **TS$_{5 \rightarrow 6}$** MO $\psi_{5 \rightarrow 6}$, highlighted in red in Figure 5 and shown also in Figure 6. Consequently, perhaps the process may be considered to be a hybrid of model A and model D in Figure 1.[27]

(23) In a few cases, some of the tiniest AO contributions had to be omitted in the transition structure bonding and antibonding MOs of Figures 5–7. All of the actual MOs can be found in Supporting Information.

(24) Cabaleiro-Lago, E. M.; Rodríguez-Otero, J.; García-López, R. M.; Peña-Gallego, A.; Hermida-Ramón, J. M. *Chem. Eur. J.* **2005**, *11*, 5966–5974.

(25) To understand why the presumed allowed rotation of the exocyclic CH$_2$ in model D of Figure 1 (with CH replacing the NH in this case) is clockwise as shown by the orbital connections, it may be instructive to view this formal $[_\pi 6_s + _\pi 2_a]$, or equivalently $[_\pi 6_a + _\pi 2_s]$ process, as a $[_\pi 2_s + _\pi 2_s + _\pi 2_a]$ one.

(26) We consider the conrotatory vs disrotatory nature of the $5 \rightarrow 6$ electrocyclization to be ambiguous at best. On the one hand, the addition of a formal antarafacial component may make it appear to be conrotatory in the way that the $_\pi 4_a$ ring closure of buta-1,3-diene is conrotatory, as compared to the $_\pi 6_s$ ring closure of hexa-1,3,5-triene **7** which is disrotatory. On the other hand, the fact that the exocyclic CH$_2$ group in **5** is predicted to rotate clockwise in model D of Figure 1 as it does in model A, may make the process best described as disrotatory.

(27) Perhaps the participation of MO $\theta_{5 \rightarrow 6}$ in **TS$_{5 \rightarrow 6}$-(8,8)CASSCF** may also be considered a secondary orbital effect, much as we consider the participation of MOs $\phi_{10 \rightarrow 11}$ and $\phi_{3 \rightarrow 4}$ in the $10 \rightarrow 11$ the $3 \rightarrow 4$ rearrangements to be.

We now turn our attention to the rearrangement of the *Z*-1-aza-1,3,5-hexatriene **9** to **11** and its orbital correlation diagram in Figure 7. In this diastereomer of 1-aza-1,3,5-hexatriene it is unlikely that the nitrogen lone-pair can play an active role in the reaction since it is pointed away from the σ-bond forming site and it may be construed from the diagram that the lone-pair orbital just rehybridizes as shown by the correlated nonbonding orbital ω and orbital ω' through **TS$_{9 \rightarrow 11}$** orbital $\phi_{9 \rightarrow 11}$ (highlighted in green). Once again, the highest occupied π-MO of **9** (χ_3) correlates with the σ-MO of product **11** (highlighted in red) as was the case for the rearrangements of **7** and **5** in Figures 4 and 5, respectively.

In the case of the rearrangement of the *E*-1-aza-1,3,5-hexatriene **10**, the nitrogen is in a position such that it could participate in the electrocyclization process, perhaps as depicted by model C in Figure 1 for the similar compound **3** (minus the terminal allenyl carbon–carbon π-bond). The orbital correlation diagram for this process in Figure 8, once again shows a χ_3-MO to σ-MO correlation through **TS$_{10 \rightarrow 11}$** MO $\psi_{10 \rightarrow 11}$ (highlighted in red). However, $\phi_{10 \rightarrow 11}$, the **TS$_{10 \rightarrow 11}$** MO that correlates the ω and ω' MOs, shows a sizable contribution from the orbital on C2 this time that partially overlaps with the lone-pair orbital on nitrogen (highlighted in green). These $\psi_{10 \rightarrow 11}$ and $\phi_{10 \rightarrow 11}$ MOs are shown fully in Figure 9 (and on page S28 of Supporting Information) and perhaps correspond, respectively, to model A and model C of Figure 1 (minus the terminal allenyl carbon–carbon π-bonds). Our interpretation of these correlations is that the electrons in χ_3-MO of Figure 8 are formally those that make the σ bond in **11**; however, given that there are contributions from the AOs on both the nitrogen lone-pair and C2 in MO $\phi_{10 \rightarrow 11}$ of Figure 8, that the lone-pair participates in a secondary orbital effect that helps stabilize the transition state of the $10 \rightarrow 11$ rearrangement.

Now that we have analyzed the results of CASSCF calculations on **5**, which has a terminal allenyl C–C π-bond but no nitrogen heteroatom, and on **9** and **10** which both have the nitrogen heteroatom but no such C–C π-bond, we turn our attention to our primary focus, the rearrangement of the 7-azahepta-1,2,4,6-tetraene **3** which has both. Figure 10 shows orbital correlations for the $3 \rightarrow 4$ rearrangement that are consistent with those for all of the other rearrangements discussed above. The highest occupied delocalized π-MO of **3**, χ_3, is once again seen to correlate only with the σ-MO of product **4** through **TS$_{3 \rightarrow 4}$** MO $\psi_{3 \rightarrow 4}$, highlighted in red, and a secondary orbital effect is seen in MO $\phi_{3 \rightarrow 4}$ (highlighted in green). These MOs are shown fully in Figure 11 (and page S20 of Supporting Information). When the results obtained on the $5 \rightarrow 6$ rearrangement are compared to those of the $3 \rightarrow 4$ one, it appears that **TS$_{3 \rightarrow 4}$-(10,9)CASSCF** has no orbital disconnection at the C2 carbon of the allenyl moiety as it appears to in **TS$_{5 \rightarrow 6}$-(8,8)CASSCF**. As mentioned above, the $5 \rightarrow 6$ rearrangement may exhibit at least some pseudopericyclic character of the type depicted in model D in Figure 1, based on its coiled geometry with a C2–C4–C5–C1 dihedral angle of 14.2° and the appearance of MO $\theta_{5 \rightarrow 6}$ shown in Figure 6. Figure 6 also shows MO $\theta_{3 \rightarrow 4}$, the corresponding MO for the $3 \rightarrow 4$ rearrangement, and it is clear from the comparison of $\theta_{3 \rightarrow 4}$ and $\theta_{5 \rightarrow 6}$ that the rather planar **TS$_{3 \rightarrow 4}$-(10,9)CASSCF** (C2–C4–C5–N7 dihedral angle −0.06°) shows none of the p orbital–allyl overlap in $\theta_{5 \rightarrow 6}$ that appears to give **TS$_{5 \rightarrow 6}$-(8,8)CASSCF** at least some pseudopericyclic character as in model D of Figure 1. Furthermore, **TS$_{12 \rightarrow 4}$-B3LYP**, with a C2–C4–C5–N1 dihedral angle of 9.4° and in which the nitrogen lone-pair orbital cannot participate

in the reaction, is more similar in geometry to **TS$_{5 \to 6}$-(8,8)CASSCF** than it is to **TS$_{3 \to 4}$-(10,9)CASSCF** (or **TS$_{3 \to 4}$-B3LYP** with C2−C4−C5−N1 dihedral angle of −0.4°). Thus the **3 → 4** rearrangement process appears to possess little, if any, of the formal characteristics of model B with two orbital disconnections, one at N1 and the other at C2, or model D with only the one orbital disconnection at C2, and may perhaps best be considered predominantly a hybrid of pericyclic model A with no orbital disconnections and pseudopericyclic model C with one orbital disconnection at N1 (cf. Figure 1). While there is apparently not a formal orbital disconnection at C2 of the allene, there may still be a role for the terminal allenyl π-bond in the reaction. Orbitals $\psi_{3 \to 4}$ and $\phi_{3 \to 4}$ of Figure 11 could be construed as involving a twisting of the allene terminus coincident with a possible hybridization of the two p orbitals on C2 involved in the C2−N1 σ-bond formation. This is quite distinct, however, from orbitals $\psi_{5 \to 6}$ and $\phi_{5 \to 6}$ shown in Figure 6 which appear unhybridized and which have been mentioned as supporting at least some character of a $[_{\pi}6_s + {}_{\pi}2_a]$ pseudopericyclic process as depicted in model D of Figure 2.

To further support these arguments, we decided to see if we could locate a hypothetical **TS$_{3 \to 4}$** that was completely planar, except for the hydrogens in the CH$_2$ group, since such a transition structure might have a better chance of being pseudopericyclic as in model B, that is, with two orbital disconnections, one at C2 and the other at N1. All the relevant dihedral angles were frozen during a (10,9)CASSCF /6-31G* transition structure optimization that was successful, giving the **Planar TS$_{3 \to 4}$-(10,9)CASSCF** structure shown in Figure 3 with zero forces and one imaginary frequency (1020 cm^{-1}). This structure is 6.8 kcal/mol higher in enthalpy (cf. Table 1) than **TS$_{3 \to 4}$-(10,9)CASSCF**, that is only 1.1 kcal/mol higher per each of the six independent dihedral angles frozen. Like transition structures **TS$_{3 \to 4}$**, **TS$_{5 \to 6}$**, **TS$_{9 \to 11}$**, **TS$_{10 \to 11}$**, and **TS$_{7 \to 8}$**, it shows a stretching vibration for the N1−C2 σ-bond being formed as well as rotation of the CH$_2$ group (cf. Figure 3). However, it obviously does not show the slight rotation of the H−N1 bond or H$_{external}$−C1 bond with respect to the N1−C2 bond being formed as did all the others. In fact, the resulting hypothetical MOs looked almost identical to the **TS$_{3 \to 4}$** ones in Figure 9, except that the individual AOs were less hybridized (i.e., more p-like) and less "tilted." (The actual MOs can be found in Supporting Information.) Thus, even when the nitrogen lone-pair orbital and the terminal C−C π-bond can line up perfectly in this hypothetical case, the reaction is apparently not pseudopericyclic with two orbital disconnections as depicted in model B, but appears more consistent with model C (cf. Figure 1).

Finally, we report results of a calculation on a version of **TS$_{3 \to 4}$** in which the plane defined by the three CH$_2$ atoms was oriented perpendicular to the plane defined by all of the other atoms in the six-membered ring, by fixing both H−C7−C2−C3 dihedral angles at 90°. The resulting structure turned out to be a second order saddle point. One of the imaginary frequencies (554 cm^{-1}) involved primarily rotation of the CH$_2$ group and the other (602 cm^{-1}) involving stretching of the N1−C2 bond being formed. Still, inspection of certain of the "MOs" it produced appears to further support our interpretation, discussed above, that the mechanism of the actual **3 → 4** rearrangement is neither purely pericyclic nor pseudopericyclic. This is because they appear to show what one would expect if the reaction were strictly pseudopericyclic as depicted in model B (Figure 1). They clearly show a mixing of the antibonding terminal allenyl C−C π-bond with the lone-pair orbital on nitrogen in both a net

bonding way (MO **16**) and an antibonding way (MO **17**). MO **16** would then correlate with the bonding σ-MO in the product and **17** with the σ*-MO and thus correspond to a pseudopericyclic process, with two orbital disconnections, as depicted in model B of Figure 1. (All MOs, including those represented by **16** and **17**, are provided in Supporting Information.)

16   **17**
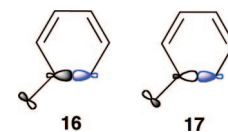
Summary and Conclusions

The normal mode vectors shown in Figure 3 for **TS$_{3 \to 4}$-(10,9)CASSCF** and **TS$_{3 \to 4}$-B3LYP** both show that there is some rotation of the N1−H group relative to the N1−C2 bond being formed, in accordance with the disrotatory motion exemplified by at least the majority of the other structures in Figure 3. The magnitude of the rotation is, however, noticeably greater in the CASSCF case (cf. **TS$_{3 \to 4}$-(10,9)CASSCF** and **TS$_{3 \to 4}$-B3LYP** in Figure 3).

As can also be seen in Figure 3, **TS$_{3 \to 4}$-(10,9)CASSCF** has a boatlike geometry similar to **TS$_{7 \to 8}$-(6,6)CASSCF**, though the former is flatter (e.g., the C3−C4−C5−N1 dihedral angle in **TS$_{3 \to 4}$** is 23.5° whereas the corresponding angle in **TS$_{7 \to 8}$** is 30.6°). While a boatlike geometry is consistent with a pericyclic transition structure, the fact that **TS$_{3 \to 4}$** is flatter than **TS$_{7 \to 8}$** argues for some pseudopericyclic character for **TS$_{3 \to 4}$**. Also, the activation barrier (B3LYP) for the **3 → 4** electrocyclization (13.9 kcal/mol) is substantially lower than that for the **12 → 4** one (24.4 kcal/mol) with a difference of 10.5 kcal/mol. This is also true for the corresponding **10 → 11** and **9 → 11** rearrangements where the difference in activation enthalpies is 16.7 kcal/mol (B3LYP) or 16.8 kcal/mol (CASSCF). These results argue for at least some pseudopericyclic character in **TS$_{3 \to 4}$** and **TS$_{10 \to 11}$** as do the 0.4 Å longer C−N π-bond lengths in **TS$_{12 \to 4}$-B3LYP** versus **TS$_{3 \to 4}$-B3LYP** and in **TS$_{9 \to 11}$-(8,7)CASSCF** versus **TS$_{10 \to 11}$-(8,7)CASSCF** (cf. Figure 3).

We have also used correlation diagrams constructed entirely from localized complete active space (CAS) MOs for the electrocyclizations of **3, 5, 7, 9**, and **10** (Figures 4, 5, 7, 8 and 10) to further explore the roles, if any, of the terminal allenyl π-bond and nitrogen lone-pair orbital in the **3 → 4** rearrangement. Our results appear to rule out a type of participation by the terminal allenyl π-bond of **3** in which there is a formal orbital disconnection at C2 (model B or model D) and suggest that it is the highest occupied delocalized π-MO of **3** that is primarily responsible for σ-bond formation in **4** (correlation involving $\Psi_{3 \to 4}$ in Figures 10). $\Psi_{3 \to 4}$, as seen in Figure 11, appears to make use of the C−N π-bond of **TS$_{3 \to 4}$**, consistent with a pericyclic process and which may be considered the primary orbital effect. However, orbital $\phi_{3 \to 4}$, as also shown in Figure 11, appears to indicate the participation of the nitrogen lone-pair orbital, essentially as depicted by model C in Figure 1, and would thus seem to argue for at least some pseudopericyclic character in **TS$_{3 \to 4}$**. On the basis of our interpretations of the orbital correlation diagrams as discussed above, we suggest characterizing the nitrogen lone-pair's participation in the rearrangement as a secondary orbital effect. In any case, the **3 → TS$_{3 \to 4}$ → 4** electrocyclization process may best be considered a hybrid of model A and model C in Figure 1, with an orbital disconnection on the nitrogen atom (N1) only, and hence neither purely pericyclic nor pseudopericyclic.[28]

Our conclusions depart from those of de Lera and Cossío[4] who appear to argue that the $3 \rightarrow 4$ rearrangement is pseudo-pericyclic involving orbital disconnections at both C2 and N1 as in model B of Figure 1. On the other hand, de Lera and Cossío's[4] finding that $TS_{3\rightarrow4}$ is less aromatic than typical pericyclic transition structures, such as $TS_{7\rightarrow8}$, is consistent with a process that is a hybrid of a pericyclic and a pseudopericyclic process.

Our results more closely parallel the conclusions of Rodriguez-Otero et al. who have argued that the electrocyclization of **3** is "essentially pericyclic," though "assisted" by the lone-pair orbital on nitrogen,[5] though "assisted" may be too weak a word to describe what appears to be a rather significant pseudopericyclic component to this rearrangement.

Supporting Information Available: Complete refs 17a and 17b. CASSCF/6-31G* optimized geometries, CASPT2/6-31G*// CASSCF/6-31G* energies, and active space molecular orbitals, including occupation numbers, for stationary points **3−11**, $TS_{3\rightarrow4}$, $TS_{5\rightarrow6}$, $TS_{7\rightarrow8}$, $TS_{9\rightarrow11}$, $TS_{10\rightarrow11}$, and a nearly planar version of $TS_{3\rightarrow4}$. B3LYP/6-31G* optimized geometries and energies for stationary points **3−12**, $TS_{3\rightarrow4}$, $TS_{5\rightarrow6}$, $TS_{7\rightarrow8}$, $TS_{9\rightarrow11}$, $TS_{10\rightarrow11}$, $TS_{12\rightarrow4}$, and a nearly planar version of $TS_{3\rightarrow4}$. Full active space orbital correlation diagrams for the $3 \rightarrow 4$, $5 \rightarrow 6$, $7 \rightarrow 8$, $9 \rightarrow 11$, and $10 \rightarrow 11$ electrocyclizations; MOs **16** and **17**, depicted schematically above; Figure 3, full page version. This material is available free of charge via the Internet at http://pubs.acs.org.

JA074402J

(28) While this manuscript was in revision, we became aware of a paper by Professor Shogo Sakai (*Theor. Chem. Acc.* DOI 10.1007/s00214-007-0312-8). He performed similar calculations on the electrocyclizations of **3**, **5**, and **12** and reached similar conclusions, though he used a CiLC-IRC approach and multiconfigurational second-order Møller-Plesset perturbation theory (MRMP), instead of CASPT2, to incorporate configuration interaction.